Energy 294 (2024) 130909

Contents lists available at ScienceDirect

Energy

journal homepage: www.elsevier.com/locate/energy

Exploring the passive the pre-chamber ignition concept for spark-ignition engines fueled with natural gas under EGR-diluted conditions

R. Novella [a], J. Gomez-Soriano [a,*], I. Barbery [a], P.J. Martinez-Hernandiz [b]

[a] CMT – Clean Mobility & Thermofluids, Universitat Politècnica de València, Camino de Vera, 46022 Valencia, Spain
[b] ITENE – Instituto Tecnológico del Embalaje, Transporte y Logística, Calle Albert Einstein 1, 46980 Valencia, Spain

ARTICLE INFO

Keywords:
Pre-chamber ignition engine
EGR dilution
Energy conversion
Jet features
Natural gas

ABSTRACT

The pre-chamber ignition system has demonstrated to be a suitable technology for increasing burning rates while reducing the cycle-to-cycle variability in spark-ignition engines. This concept offers an improvement in thermal efficiency through an increase in ignition energy and flame surface, allowing it to overcome knocking combustion issues at high engine load/speeds. This fact makes this ignition concept well compatible with the use of dilution strategies to control emissions or to further improve efficiency. However, despite promoting faster combustion, knocking combustion is still a major limitation at low rotational speeds and high engine loads (low-end torque). In this investigation, the performance of the passive pre-chamber concept is evaluated in a single-cylinder turbocharged spark-ignition engine fueled with compressed natural gas in EGR-diluted conditions. Several experiments and numerical simulations are combined to analyze the basis of the pre-chamber operation, while seeking to improve the global performance of the engine. To this end, a new pre-chamber geometry is proposed that is able to achieve better features in the ejected jets, to enhance the performance of the concept in the whole engine map.

1. Introduction

Traditionally, knocking combustion has been considered the main constraint for increasing efficiency in spark-ignition (SI) engines [1,2]. As the unburned mixture region downstream of the flame auto-ignites, an abnormal and uncontrolled combustion appears, suddenly increasing the pressure gradients within the cylinder [3] and, consequently, compromising the integrity of the combustion chamber. This problem can be seen as a kind of race, where the flame initiated by the spark must sweep the combustion chamber volume completely before the auto-ignition delay time (AID) of the unburned mixture is reached. To prevent knock, some strategies focus on increasing the burning rate [4,5], while others focus on extending the auto-ignition delay of the unburned mixture through knock-resistant fuels [6,7] or dilution strategies based on exhaust gas recirculation (EGR) [8,9].

The pre-chamber ignition system [10,11], also known as Turbulent Jet Ignition (TJI), increases the burning rates by initiating combustion at different locations inside the combustion chamber with highly turbulent jets of hot products [12,13]. Consequently, the combustion phasing can be optimized to reach a higher thermal efficiency in operating conditions where knocking combustion impedes further advances of the spark timing [14,15].

This ignition strategy can be implemented by two different approaches: active [16,17] and passive (or unscavenged) systems [18,19]. The active system uses a dedicated fuel injector inside the pre-chamber [20,21] that keeps the air-to-fuel mixture at optimum values for combustion (close to stoichiometric conditions) [22]. The passive system is a simplified configuration without this secondary fuel injector [23], which reduces the assembly and packaging costs, making it an attractive alternative for passenger car applications.

The interest of this ignition system has been demonstrated by the number of investigations conducted during the last decade. Mastorakos et al. [24] studied the fundamental aspects of jet ignition through both experiments and simulations. Allison et al. [25] and Bunce et al. [26] investigated the effect of the pre-chamber configuration on the jet dynamics and combustion physics. Moreover, the synergies between pre-chamber ignition and other strategies proposed to improve the engine thermal efficiency, such as lean burn and the use of hydrogen, have been evaluated in previous studies by Benejes et al. [27,28]. Furthermore, the effect of nozzle diameter and pre-chamber volume on combustion performance was also investigated by Thelen et al. [29], Biswas et al. [30,31] and Onofrio et al. [32].

More recently, investigations of the pre-chamber ignition concept implemented in natural gas engines have been conducted by Yang

* Corresponding author.
E-mail address: jogoso1@mot.upv.es (J. Gomez-Soriano).

https://doi.org/10.1016/j.energy.2024.130909
Received 7 July 2023; Received in revised form 21 February 2024; Accepted 3 March 2024
Available online 4 March 2024

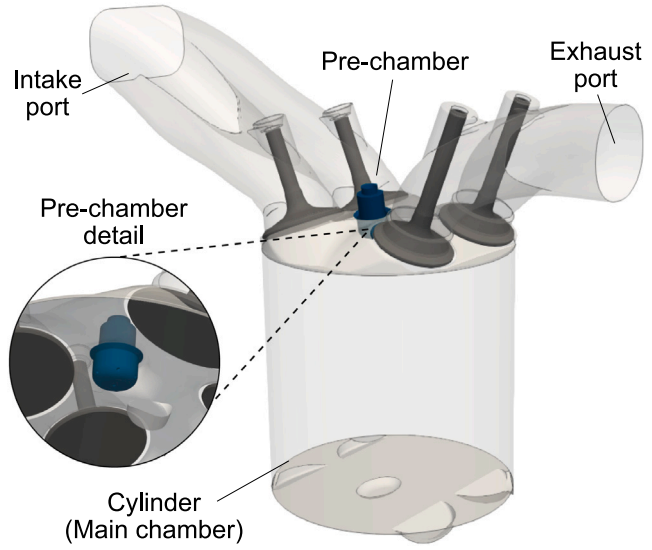

Fig. 1. Outline of the pre-chamber and combustion chamber design including the intake and exhaust ports geometry.

et al. [33], Kim et al. [34], Zardoya et al. [35,36] and Payri et al. [37]. Furthermore, the use of the pre-chamber system to extend the EGR dilution tolerance for improving the engine thermal efficiency and controlling output emissions has also been the focus of recent studies [38,39].

However, several of these research works have proven that the pre-chamber ignition system, especially in its passive form, operates differently across the engine map [40]. For instance, some investigations reported that the highest increase in thermal efficiency occurs at high load/speed conditions when compared to the conventional SI system [15,41,42]. In addition, one of the main constraints of the concept has been reported at low engine loads, where the pre-chamber system loses performance and it is unable to achieve a suitable spark-timing delay for catalyst activation [43]. Moreover, there is still an important knowledge gap regarding the pre-chamber performance in one of the most critical regions of the engine map, the operation at high load and low engine speed (low-end torque region).

Thus, considering the issues reported in the literature regarding the pre-chamber ignition system, this paper evaluates the use of EGR-dilution strategies to overcome the highlighted shortcomings. The investigation is focused on describing the real performance of the concept in the most critical conditions, emphasizing the key aspects and main limitations of this ignition strategy in different regions of the engine map. To this end, an extended experimental campaign combined with numerical simulations was performed on a turbocharged Miller-cycle SI engine fueled with compressed natural gas (CNG) and using EGR dilution. This method allowed for the assessment of the performance of the concept by examining the fundamental aspects, such as the ejection process during pre-chamber combustion, while evaluating the impact of pre-chamber geometry.

The paper is organized as follows: In addition to the introduction presented in this section, Section 2 describes the experimental and numerical tools utilized. Section 3 outlines the methodology followed in the investigation. Section 4 presents a comparison between the conventional SI and the pre-chamber ignition systems, along with an optimization of the pre-chamber design.

2. Experimental and numerical tools

2.1. Engine architecture and test cell characteristics

A single-cylinder version of a 4-stroke turbocharged spark-ignition engine has been used as the research platform. The main specifications of the engine are summarized in Table 1. The cylinder head is equipped with four valves with double-overhead camshafts. The fuel injection system originally developed for gasoline direct injection (GDI) has been removed. A port fuel injection (PFI) system was used instead to ensure the homogeneity of the air-fuel mixture. The valve overlap has been completely removed to prevent short-circuit losses and a Miller cycle configuration was chosen to reduce pumping losses.

Table 1
Main specifications of the engine.

Engine	4-stroke SI
Number of cylinders [-]	1
Displacement [cm^3]	404
Bore – Stroke [mm]	80.0–80.5
Compression ratio (geometric) [-]	15.4:1
Valvetrain [-]	DOHC
Number of valves/cylinder [-]	2 intake and 2 exhaust
Fuel injection system [-]	PFI (p_{max} = 6 bar)

Table 2
Main specifications of the reference pre-chamber ignition system.

Unscavenged pre-chamber	
Volume [mm^3]	600
Height [mm]	15.8
Hole diameter [mm]	0.7
Hole area [mm^2]	2.3
Number of holes [-]	6
Hole tangential angle [deg]	7.5

Table 3
Main specifications of the fuel.

Type	CNG RON120
H/C ratio [mol/mol]	3.84 mol/mol
O/C ratio [mol/mol]	0.0 mol/mol
Oxygen content [%]	0.0
A/F_{st} [-]	16.72
Lower Heating Value (LHV) [MJ/kg]	48.931
Density (15°C) [kg/m^3]	5
Reduced formula ($C_xH_yO_z$)	1.077 (x) - 4.137 (y) - 0.0 (z)

The housing in the cylinder head is shared between both ignition systems (conventional spark plug and pre-chamber ignition), allowing for a fast and straightforward exchange. This is located between the intake and exhaust valves as shown in Fig. 1. The system is a passive (unscavenged) pre-chamber configuration with the specifications presented in Table 2. Experiments were performed using calibrated compressed natural gas (CNG) fuel with characteristics as shown in Table 3.

A simplified outline of the test cell is depicted in Fig. 2. An external compressor is utilized to provide the necessary airflow in boost conditions. The exhaust back pressure is regulated with a throttle valve located in the exhaust line. A low-pressure EGR system is installed to provide the desired cooled EGR, which is compatible with operation at high intake boost pressures. An AVL 577 conditioner, independent from the engine, controls oil and water temperatures. Fuel consumption is measured by a BRONKHORST F-113AC-M50-AAD-44-V flowmeter.

The test cell equipment also includes a HORIBA MEXA 7100 DEGR gas analyzer, which measures pollutant emissions originating from engine operation. The analyzer is installed close to the exhaust settling chamber to obtain adequate measurement temperatures. The main emissions measured include O_2, CO, CO_2, HC, and NO_x. An AVL 415 Smokemeter is utilized to measure soot emissions traced by the filter smoke number (FSN).

Instantaneous intake and exhaust pressures are measured by piezo-resistive sensors, while in-cylinder pressure is measured by a piezoelectric sensor. The high-frequency signals are sampled with a resolution of 0.2 cad. The air-to-fuel ratio is estimated using different methods: a

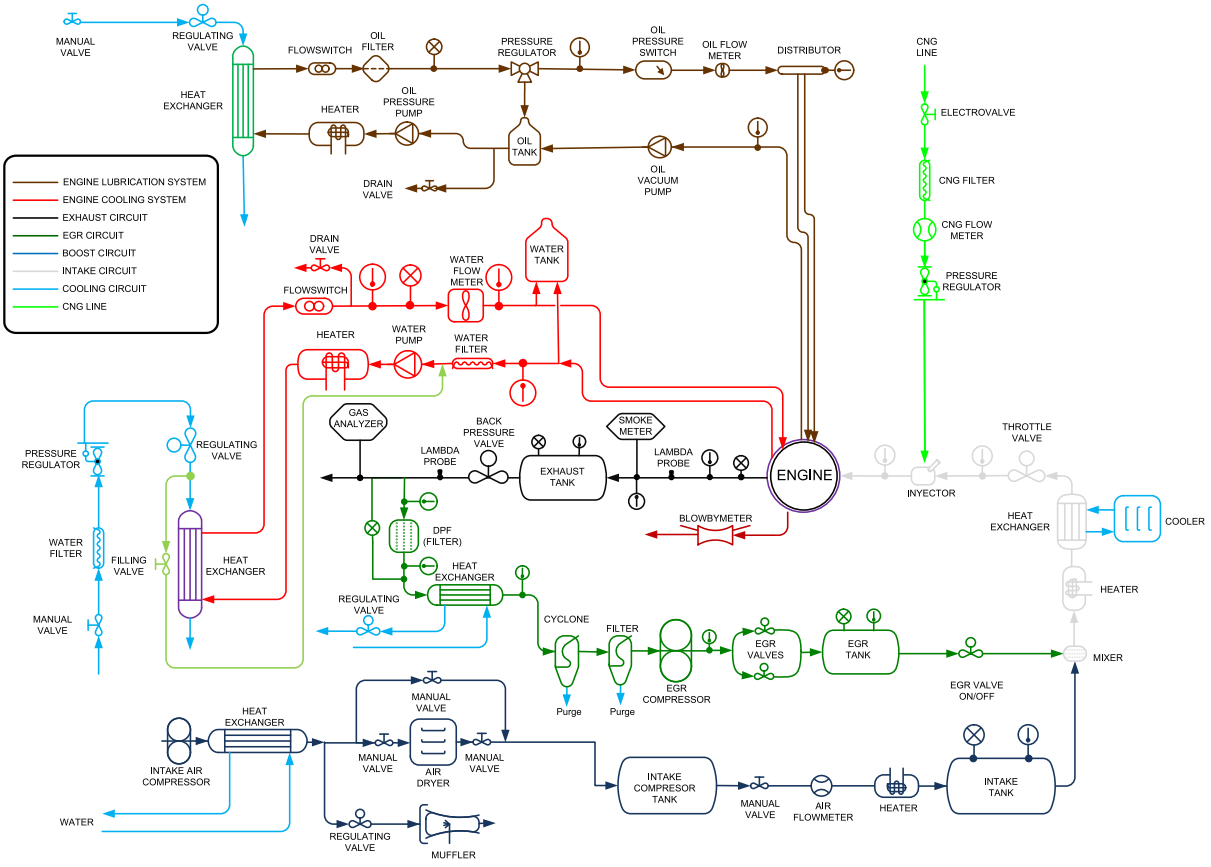

Fig. 2. Layout of the engine test cell.

lambda sensor located at the exhaust line, the gas analyzer, and computation involving the fresh air mass flow rate and the total injected fuel mass flow rate (excluding the residual air present in the EGR).

The most relevant parameters related to combustion, such as indicated gross mean effective pressure (IMEP), start of combustion (SoC), combustion phasing (CA50), combustion duration (CA1090), maximum cylinder pressure, combustion stability, heat release rate (HRR), and cylinder mean gas temperature, are calculated from the cylinder pressure signal by an in-house 0D combustion diagnostics software [44,45].

2.2. Virtual engine model

A virtual engine model is used to complement the experiments. Full details of the model setup are explained in previous publications by the authors [15,43]. The pre-chamber ignition system coupled to the combustion chamber is modeled by connecting two engine cylinders through a series of nozzles that mimic the pre-chamber holes. Intake and exhaust lines are removed, simulating only the closed-volume part of the engine cycle. this helps to considerably reduce the calculation time while retaining relevant information during the ejection process (i.e. flow velocity, mass flow rate and species concentration).

The pressure and temperature at the start of each simulation are obtained from the combustion diagnosis tool. Similarly, the combustion process in the main chamber is modeled by imposing the HRR obtained from the experiments. The heat release rate in the pre-chamber is simulated using a Wiebe function. To define the combustion phasing of the pre-chamber, 50% of the pre-chamber combustion is fixed at the start of the main chamber combustion. This represents the main uncertainty of the model; as there is no possibility of measuring the pressure inside the pre-chamber, this value has been estimated from the literature. The lengthening effect on combustion duration when adding EGR in the pre-chamber is simulated by imposing the same increment of combustion duration as in the main chamber.

The virtual model was accordingly calibrated and validated against experiments performed on the bench. Given that the HRR in the main chamber is directly imposed from the experiments, the only variable requiring validation is the instantaneous in-cylinder pressure. Consequently, the calibration process is focused on adjusting the constant of the heat transfer model between the fluid and the solid surfaces. Results of the validation under high engine load and speed conditions (Point 14, HLHS) can be found in [15], while further validation under low engine load and speed (Point 1, LLLS) can be found in [43]. Additionally, Fig. 3 displays the validation results of two additional points, which are relevant for this particular investigation. Blue lines correspond to Point 16 (HLLS), and orange lines correspond to Point 12 (LLHS). Solid lines represent the experimental pressure in the main chamber, while dashed lines symbolize the simulated ones. These results demonstrate the robustness of the virtual engine model in reproducing the experimental trends.

2.3. 1-D jet model

The virtual engine model is coupled with an in-house 1-D jet model. This code estimates the characteristics of a gaseous jet injected into a controlled environment. The model predicts the jet tip penetration, cone angle, and species concentration based on the outputs of the virtual engine model (such as jet momentum, mass flow rate, and main chamber density). The main assumptions and the fundamental modifications required to adapt the original model (initially developed for diesel injection) to pre-chamber gas ejection are explained in [46]. Moreover, comprehensive details of the original model are provided in [47–49].

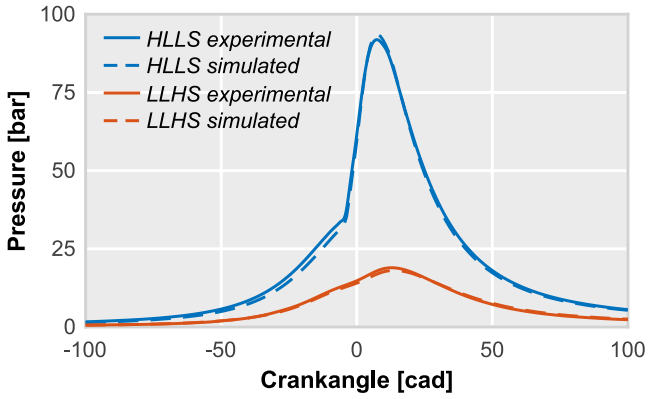

Fig. 3. Validation results of the virtual engine model. Experimental and simulated pressure profiles in the main chamber for Point 16 (also denoted as HLLS) and Point 12 (LLHS).

3. Methodology

To evaluate the effect of EGR on pre-chamber operation, a series of operating conditions were specifically chosen to cover the entire engine map, with a special emphasis on the low-end torque region (high-load/low-speed). Therefore, the experimental campaign consisted of 21 operating points, each characterized by a pair of engine speed and load conditions. Full details of these points are presented in Table 4. The first set of experiments (points 1 through 14) was measured considering three different scenarios: conventional SI without external EGR, pre-chamber ignition without external EGR, and pre-chamber ignition with external EGR addition. The first two scenarios were measured to establish a reference from which a solid comparison can be made. The final set of experiments (points 15 through 21) was only measured in the third scenario, where the pre-chamber ignition system is combined with external EGR. These operating conditions could not be measured in the other two situations because of limitations due to knocking combustion (in the case of conventional SI) or combustion instabilities (in the case of PC ignition).

The target indicated mean effective pressure (IMEP) was fixed by a reference injected fuel mass when operating with the conventional SI system. In this conditions the spark timing was adjusted to reach maximum brake torque (MBT) conditions. Then, the fuel injected mass was kept constant when changing the ignition system to keep the fuel energy between equivalent tests. Regarding EGR-diluted tests, a similar methodology was followed, increasing the dilution ratio in steps of 5% up to reaching the maximum efficiency point while maintaining a stoichiometric mixture.

Additionally, the experimental data are combined with the numerical tools described in the previous section. The virtual engine model and the 1-D jet model were coupled with the objective of analyzing the performance of the pre-chamber ignition system in terms of jet features. This combination showed promising results in previous research works [46,50] and will help propose guidelines for pre-chamber design that improve engine performance in the whole operating map.

4. Results and discussion

This section presents and discusses the main findings of this investigation. First, a comparison between the conventional SI system and the passive pre-chamber concept is presented, considering also external EGR addition for the pre-chamber ignition cases. Based on this analysis several 0D/1D simulations were performed in order to study the energy conversion inside the pre-chamber, and propose some design solutions to improve the performance of the ejected jets. Finally, a discussion about the advantages and drawbacks of the passive pre-chamber ignition concept in the different areas of the engine map is presented.

Table 4
Operating conditions measured.

	IMEP [bar]	Engine speed [rpm]	Ignition system [-]	EGR [–]
Point 1 (LLLS)	3.50	1250	SI/PC	w/wo
Point 2	10.0	1250	SI/PC	w/wo
Point 3	8.50	1750	SI/PC	w/wo
Point 4	12.0	1750	SI/PC	w/wo
Point 5	3.50	2000	SI/PC	w/wo
Point 6	8.50	2000	SI/PC	w/wo
Point 7	13.6	2000	SI/PC	w/wo
Point 8	6.00	2500	SI/PC	w/wo
Point 9	12.0	2500	SI/PC	w/wo
Point 10	3.50	3000	SI/PC	w/wo
Point 11	8.50	3500	SI/PC	w/wo
Point 12 (LLHS)	3.50	4000	SI/PC	w/wo
Point 13	13.3	4000	SI/PC	w/wo
Point 14 (HLHS)	14.0	4000	SI/PC	w/wo
Point 15	11.0	1250	PC	w
Point 16 (HLLS)	14.0	1250	PC	w
Point 17	11.4	1500	PC	w
Point 18	12.5	1500	PC	w
Point 19	15.0	1500	PC	w
Point 20	15.0	1750	PC	w
Point 21	15.0	2000	PC	w

4.1. Conventional SI system vs passive pre-chamber ignition

To start with the comparison, the gross indicated efficiency obtained along the whole engine map is shown in Fig. 4. Here, three different scenarios are considered operating at stoichiometric conditions: conventional SI and pre-chamber ignition with and without EGR addition.

Focusing on the conventional SI system and the pre-chamber ignition comparison, it can be seen that the pre-chamber ignition concept does not improve the performance of the conventional SI system. Indeed, it worsens efficiency levels in the low engine speed range significantly. While these values are similar above 2500–3000 rpm, they notably decrease below 2000 rpm. For instance, the gross indicated efficiency drops from 38.8% to 35.5% in Point 1 (1250@3.5) and, from 39.4% to 36.4% in Point 2 (1250@10).

As it can be seen in the bottom graph of Fig. 4, the situation is completely different when including EGR in the equation. Here, the dilution level (EGR) was targeted to maximize the gross indicated efficiency at each operating point. The specific values of EGR dilution are shown in Fig. 5 for reference. The efficiency levels improve in all the points considered except in Point 12 (4000@3.5), which is actually of limited relevance from the engine operation point of view (real driving cycles show a very low operating density under these conditions [51]). In addition to this generalized increase in efficiency, the operating range can be extended beyond the limits set by knocking combustion. Points from 15 to 21 can be measured thanks to the combination of pre-chamber ignition and external EGR, demonstrating competitive efficiency values even under these extreme conditions.

This increase in operating range coincides with the points where the external EGR amount reaches the higher values along the operating map. Fig. 5 shows that EGR should be increased as the engine load rises and the engine speed decreases to reach the maximum thermal efficiency.

In order to dig into the root cause of this particular behavior, the combustion phasing of the three scenarios is depicted in Fig. 6. The conventional SI ignition is able to trigger the combustion at suitable values in the whole engine map (from 6 to 11 CAD aTDC), finding a reasonable range between knocking and unstable combustion. The pre-chamber ignition operated without external EGR, shows similar values of combustion phasing along the engine map, except for the low-speed/high-load zone. Here, combustion must be triggered before TDC to avoid excessive CCV. In these conditions, the drop of turbulence

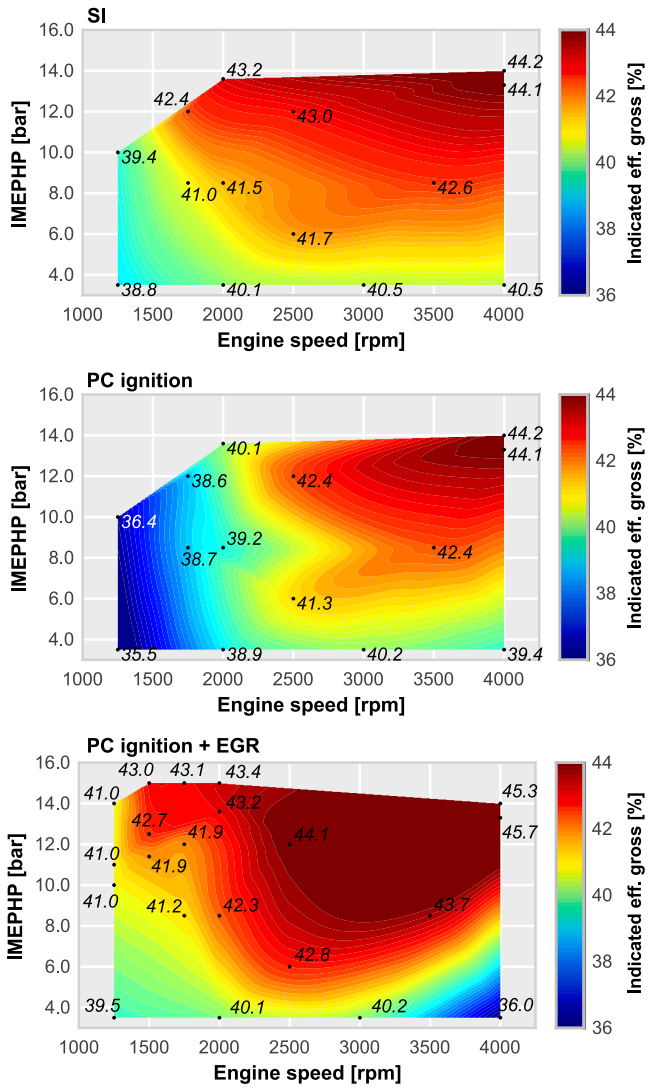

Fig. 4. Gross indicated efficiency maps for the conventional SI system (top), passive pre-chamber ignition system no EGR (middle) and passive pre-chamber ignition system with EGR (bottom).

and flow velocity inside the pre-chamber compromises the combustion stability [52], reducing flexibility in optimizing combustion phasing. This is reflected in the loss of efficiency observed in Fig. 4 (middle).

Adding external EGR seems to help in this situation, the dilution of the mixture extends the duration of combustion allowing an optimum phasing which maximizes the engine efficiency. In addition, the turbulence intensity drop and the flow velocity decline inside the pre-chamber is compensated, widening the operating range in these critical conditions. The engine load can be increased up to values of 15 bar of IMEP at engine speeds below 2000 rpm keeping reasonable efficiency levels.

In order to understand the fundamental aspects of these trends, a set of simulations were carried out using the virtual engine model. Figs. 7 and 8 show the fuel mass available at the start of ejection and the maximum HRR peak achieved inside the pre-chamber in both situations: with and without EGR.

In general, the available fuel inside the pre-chamber increases with the engine load due to the larger amount of injected fuel. The maximum HRR inside the pre-chamber is also affected by the engine load and speed, however this correlation is not so evident. In contrast to the PC fuel mass trends, the maximum values of HRR are focused in the

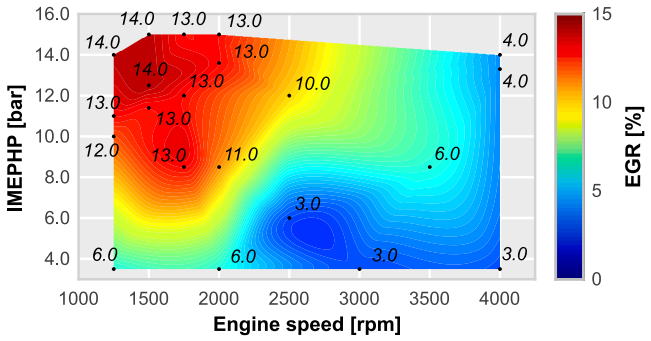

Fig. 5. EGR dilution values used in the stoichiometric tests of the pre-chamber ignition concept.

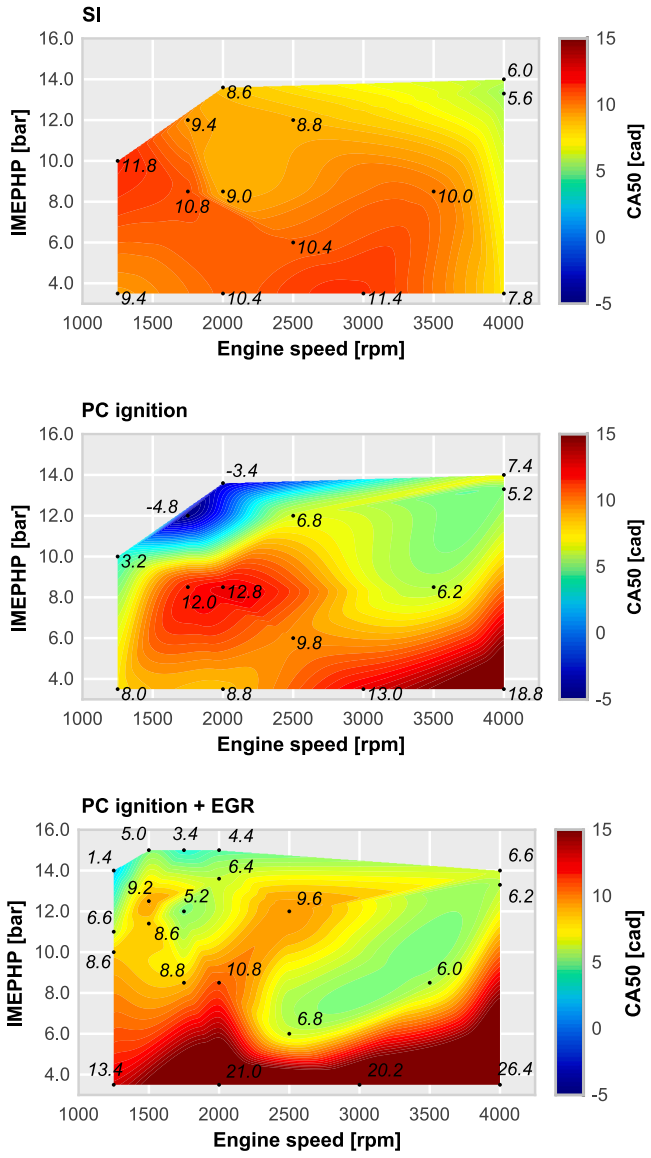

Fig. 6. Combustion phasing maps (CA50) for the conventional SI system (top), passive pre-chamber ignition system no EGR (middle) and passive pre-chamber ignition system with EGR (bottom).

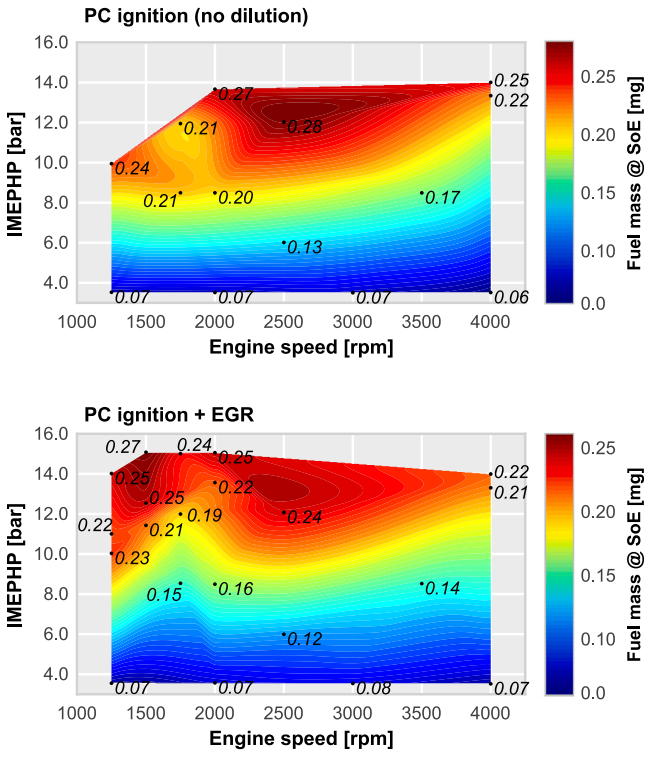

Fig. 7. Estimated fuel mass inside the pre-chamber at start of ejection (SoE) for the TJI concept operating without EGR (upper) and with EGR (bottom) at $\lambda = 1$.

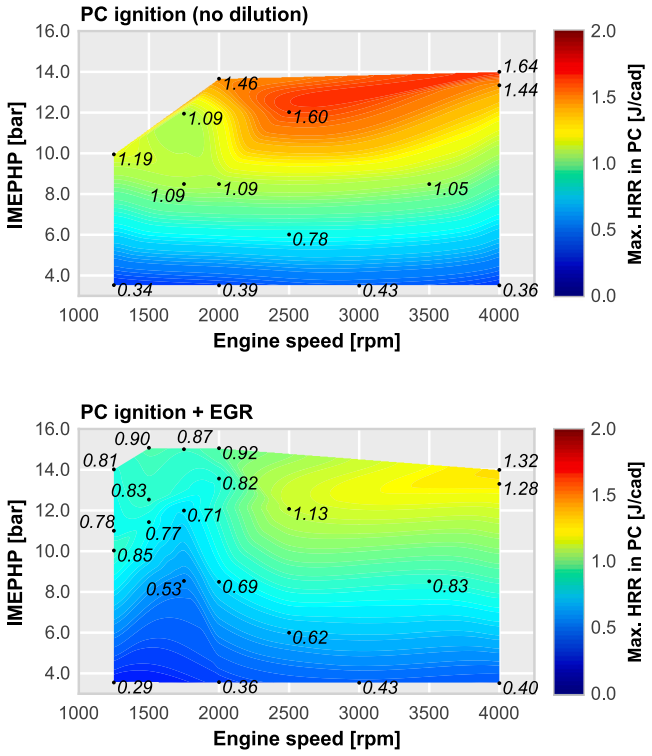

Fig. 8. Estimated maximum combustion velocity peak inside the pre-chamber for the TJI concept operating without EGR (upper) and with EGR (bottom) at $\lambda = 1$.

high speed and load zone, avoiding the high load and low speed regime. Moreover, the addition of EGR has a remarkable effect on

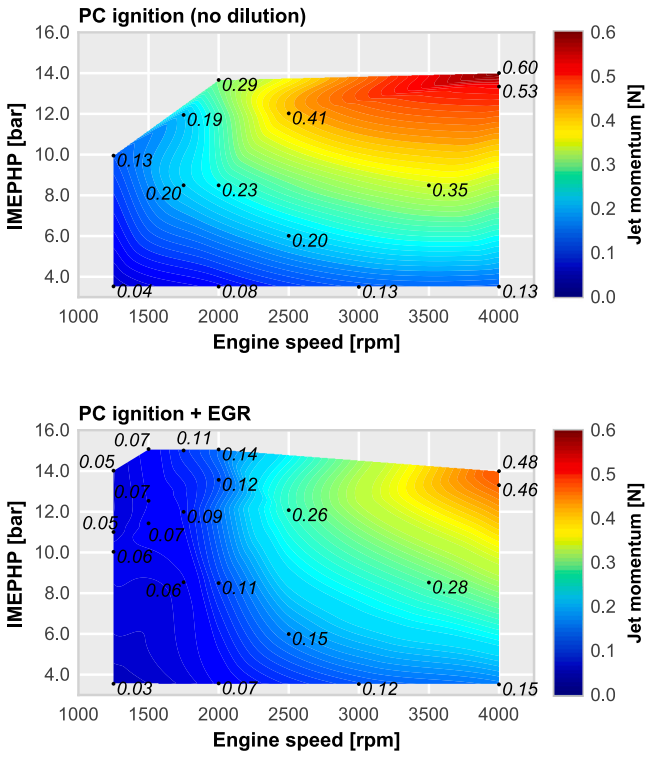

Fig. 9. Maps of maximum jet momentum flux for the TJI concept operating without EGR (upper) and with EGR (bottom) at $\lambda = 1$.

both parameters. The increased combustion duration caused by EGR addition reduces the maximum HRR peak inside the pre-chamber in the whole engine map. Due to this effect, combustion in the pre-chamber should start earlier to maintain a suitable MC combustion phasing, thereby conditioning the PC filling. However, it can be seen that the mass inside the PC is hardly affected in spite of the spark timing advance. This is demonstrated by comparing some of the equivalent operating points (i.e. Point 2, 4 and 7), where the mass changes from 0.24 to 0.23 mg, 0.21 to 0.19 mg and 0.27 to 0.22 mg respectively.

At this point, it is not evident which is the controlling parameter of the process, as there is no answer to why the EGR helps to increase the operating range and improve the efficiency of the concept. The analysis of the pre-chamber pressurization is the next step in the investigation, due to its relationship with the jet momentum flux that has been shown to be crucial to the concept performance in a previous publication [50].

The 1-D jet model simulations provided the jet momentum estimation presented in Fig. 9. Examination of these maps evinces the relationship between the momentum flux of the jets and the burning rate inside the PC already displayed in Fig. 8. The comparison of the low-end torque region (Point 16 or HLLS) against the maximum power region (Point 14 or HLHS) when operating with EGR confirms this connection. While the fuel mass is in the same range (0.26 mg versus 0.22 mg), the maximum HRR peak is almost 60% higher (0.92 J/cad versus 1.32 J/cad). This results in a difference of almost 0.4 N in terms of jet momentum; almost 9 times higher for the HSHL point. Focusing on the low load engine region, the same trend is observed. There is an increment in the resulting jet momentum as increasing the engine speed while keeping the same gross IMEP. These trends are also observed in the non diluted case at a lower extent, but confirming the link between the burning rate inside the PC and the jet performance.

Although the trends across the map are similar, there is a generalized decrease in the jet momentum values for the EGR case. This is difficult to understand considering the findings of the previous research [50]. This investigation shows how pre-chamber designs that

Table 5
Main specifications of the optimized pre-chamber designs.

Parameter	Reference	HLLS opt.	HLHS opt.	LLLS opt.	LLHS opt.	Compromise design
Volume [mm^3]	600	2000	2000	2000	2000	2000
Height [mm]	15.8	52.7	52.7	52.7	52.7	52.7
Hole diameter [mm]	0.7	0.6	2.8	0.8	2.8	0.9
Hole area [mm^2]	2.3	1.6	12.0	2.78	12.0	4.0
Number of holes [-]	6	6	6	6	6	6
Hole tangential angle [deg]	7.5	7.5	7.5	7.5	7.5	7.5

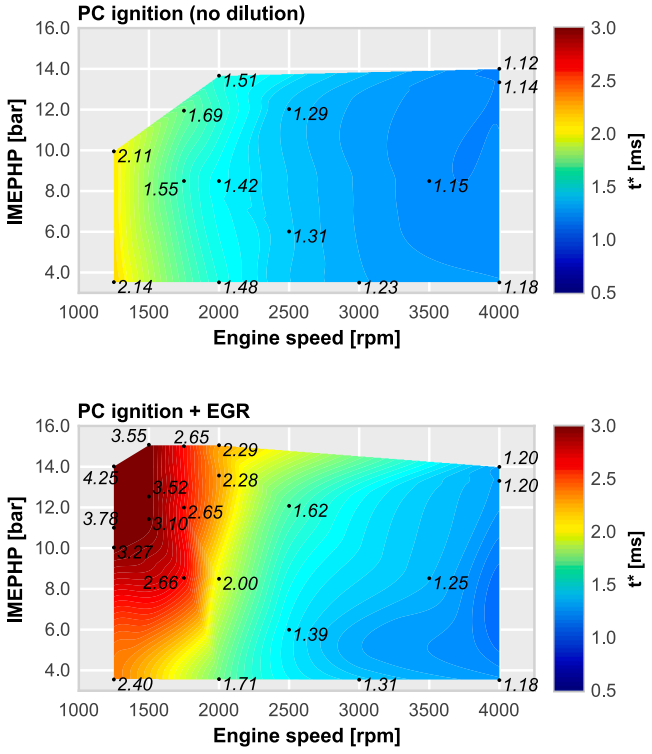

Fig. 10. t*-maps for the TJI concept operating without EGR (upper) and with EGR (bottom) at $\lambda = 1$.

promote higher momentum values in the jets improve the performance of the concept under non-dilution conditions as they significantly influence the initial ignition surface of the main chamber. In addition, the relationship between the ignition surface and the time to reach the farther wall, or what the authors call "t*", is widely explained. As described in previous sections, the 1-D jet model estimates the transient penetration of a free jet using the diameter of the nozzle hole, the effective ejection velocity profile (derived from the momentum and mass flow rate profiles), and the downstream thermodynamic conditions in the main combustion chamber. Based on this information, the model calculates the time required for the jet to reach the cylinder wall by comparing it with the geometrical characteristics of the main chamber. The authors advocate that a shorter t* translates into a larger ignition surface and a shorter delay between the PC and the MC, leading to an improved performance of the concept.

In order to better understand this behavior when considering EGR dilution, the calculated values of t* are presented in Fig. 10. As it can be expected, t* (expressed in ms) is related with the engine speed. They exhibit similar values for engine speeds above 2000 rpm between non-diluted and EGR-diluted cases. However, the EGR case shows significantly higher values for the engine speeds gathered by 1250 rpm and 2000 rpm, being precisely the range that offers the greater efficiency gains of the concept.

As opposed to the non-dilution case where more jet surface equals enhanced performance, the EGR case does not exhibit a clear relationship. Obviously, more ignition area is advantageous for the main chamber burning, but the relationship with the conditions in the pre-chamber negatively affects the operation stability. Therefore, the key aspect is not to generate good jets but to be able to maintain combustion in the pre-chamber, which at least guarantees an ejection of hot gases towards the MC.

In summary, the addition of external EGR helps in extending the operating range while improving the engine efficiency in particularly interesting conditions from a real driving conditions point of view. However, the reduction of the HRR inside the pre-chamber caused by the diluted mixture deteriorates the resulting jet momentum and thus, the overall performance of the concept. This opens the way for a possible optimization of the pre-chamber design that further improves the concept.

4.2. Pre-chamber design optimization

In view of the possibilities observed in the previous section, the basic configuration of the pre-chamber design is optimized for EGR operation using the numerical methodology proposed by Novella et al. [50]. To this end, only the four extreme conditions labeled by LLLS (1), HLLS (16), LLHS (12) and HLHS (14) in Table 4 are considered.

This method is based on a series of simulations using the virtual engine model. A design of experiments (DoE) using the pre-chamber volume and nozzle orifice diameter as optimization parameters was performed. The PC volume was swept between 400 mm^3 and 2000 mm^3. The orifice diameter, studied through the total cross sectional area and considering the same number of nozzles (6), was ranged from 0.75 mm^2 to 12.0 mm^2. In both cases, the ranges are limited by structural or manufacturing constraints.

The resulting estimations of t* for the four operating points considered are presented in Fig. 11. Here, the jets performance along the sample space can be easily analyzed. Black lines represent the combination of parameters that gives the same t* value obtained with the reference pre-chamber (Table 2). And, the black square point represents the optimum pre-chamber geometry at that operating condition, that is the one with the lowest t*.

Results show a reduction of t* values as the pre-chamber volume increases in all operating points. This is related to the larger amount of fuel available inside the pre-chamber that allows to increase the maximum HRR peak and subsequently resulting in higher jet momentum values. In terms of total nozzle area, there are two different ways to optimize the PC depending on the engine speed. It can be observed that larger nozzle diameters reduce the t* at high engine speed. As the time gap for the pre-chamber filling is considerably reduced at these conditions, large orifices ensure optimal PC filling avoiding excessive friction losses through the nozzles. For low engine speeds, narrower nozzles exhibit the lowest t* values. Here, the PC filling is not constrained by time restrictions then, small nozzles guarantees a suitable PC pressurization and higher jet velocity.

It is clear that there is no single optimum pre-chamber design for all operating points. However, looking at the numbers, a compromise solution can improve the performance of the reference system significantly. In order to choose the best configuration, Fig. 12 overlaps the optimum

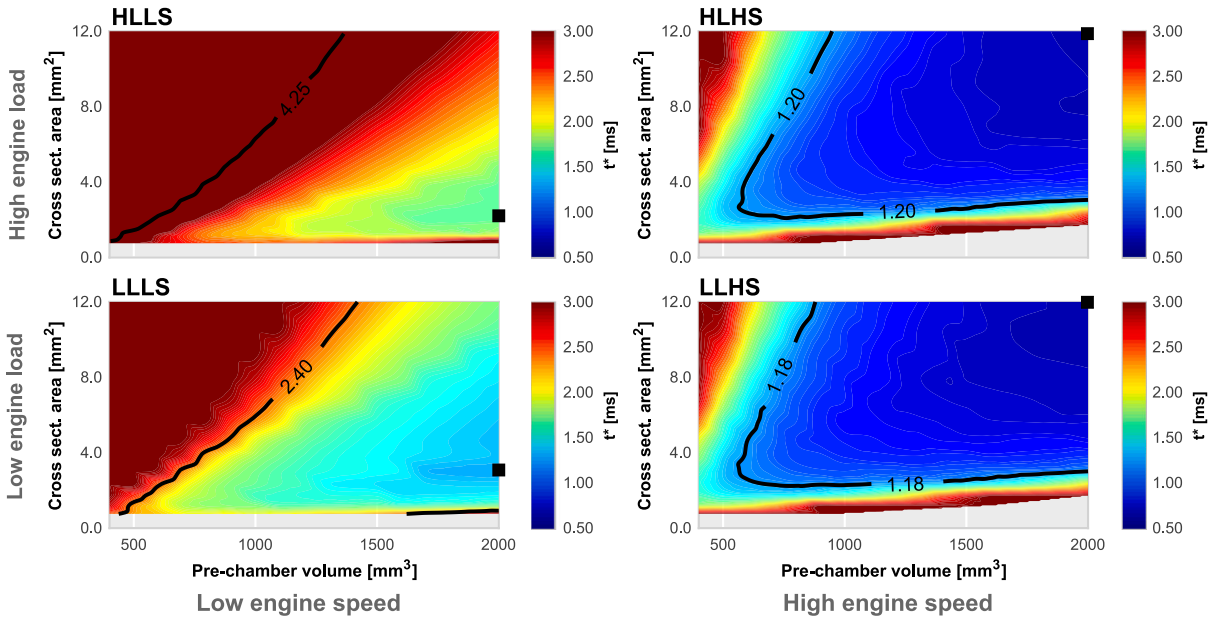

Fig. 11. Results of the PC design optimization methodology. The maps of t* for the extreme operating points.

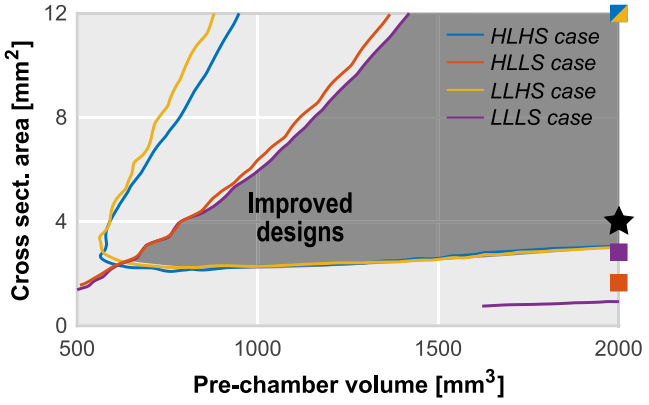

Fig. 12. Optimized space. The optimum configuration zones are overlapped together with the best pre-chamber configuration at each extreme operating point (square points).

areas identified in Fig. 11. In addition, The optimum configurations for each operating point are included for reference (square points).

In this figure, the lines intersection indicates the geometrical limits of the pre-chamber that performs, at least, as the reference pre-chamber. Thus, the proposed PC design should be located in the highlighted area that gathers larger volumes and nozzles than the reference PC. The black star represents the pre-chamber geometry selected as a compromise solution for all the operating points considered. This configuration consists of a high volume PC (2000 mm^3) and medium/small nozzles (4.00 mm^2). The latter parameter was chosen to deal with the optimum t* values region at HLLS and LLLS points.

In order to provide insight into how the pre-chamber design changes while maintaining the most restrictive geometric specifications, a conceptual exercise has been proposed to recalculate the non-constrained geometric parameters. To this end, the internal diameter of the pre-chamber was kept at the reference value since the spark plug housing has limited access and the spark plug metrics are standard. Additionally, the number and orientation of the nozzles were also maintained to sweep the main chamber similarly while avoiding excessive torching of wall surfaces. The resulting PC parameters are summarized in Table 5.

As a final step, the compromise PC design was simulated at all operating points to quantify the possible gains along the whole operating map. Fig. 13 shows the relevant parameters analyzed so far considering the new pre-chamber. Results of this figure will be compared with those obtained in the previous section for the reference PC system with EGR (Figs. 7, 8, 9 and 10). To avoid confusion and due to visualization issues, note that the color scale in these figures does not necessarily match.

As it can be seen, the fuel available inside the PC at the ejection start is substantially larger in the new pre-chamber configuration, especially at HLLS conditions. In this region of the map, it is possible to identify values three times higher than the reference ones. Similarly, there is a noticeable increment of maximum HRR peak in the whole map. In this case, the increase is generalized throughout the operating map. In both parameters, trends are similar when comparing the reference with the new PC design. They better correlate with the engine load rather than the engine speed.

As expected, the jet momentum for the new pre-chamber configuration also improves respect to the reference one in the whole engine map. This increment is caused mainly by the increased HRR, as the general trends of both maps are quite similar. Again, the region of HLLS is the most improved, as it exhibit values around 5 times higher than those obtained with the reference PC. Finally, results of t* evince the significant performance improvement expected with the new pre-chamber. In this regard, it can be seen that the new PC improves performance over the whole engine map despite having been optimized at only four extreme points.

In order to quantify the possible gains in the concept performance in the hypothetical case that the pre-chamber could be optimized independently for each operating point, Fig. 14 compares the t* values obtained with the compromise PC and the optimum one in each of the 4 extreme operating points of the map. In addition, the values calculated with the reference pre-chamber are included. As we have seen, the improvement over the reference PC is substantial. However, there is not a large difference between the compromise pre-chamber and the optimum ones, highlighting the potential of the proposed PC design to optimize the concept in diluted conditions.

5. Conclusions

The passive pre-chamber ignition concept has been experimentally and numerically evaluated in a turbocharged high compression ratio

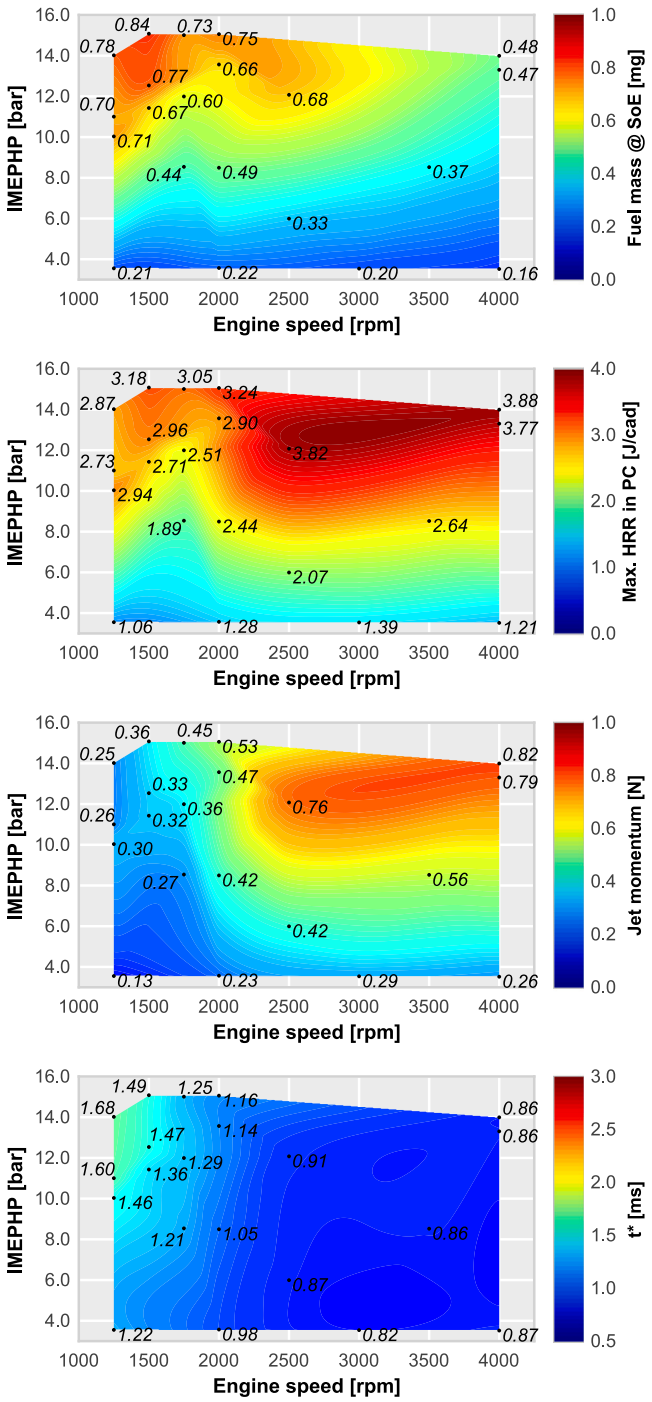

Fig. 13. Maps of fuel available inside the pre-chamber (a), maximum HRR peak (b), jet momentum flux (c) and t* (d) for the new pre-chamber configuration.

Miller-cycle engine fueled with compressed natural gas at multiple operating conditions.

Results showed that the pre-chamber ignition concept does not improve the performance of the conventional spark-ignition system. Indeed, the main limitations of the concept arise at high engine load and low engine speed conditions where efficiency levels are significantly worse. Here, the drop of turbulence and flow velocity inside the pre-chamber compromises the combustion stability, reducing flexibility

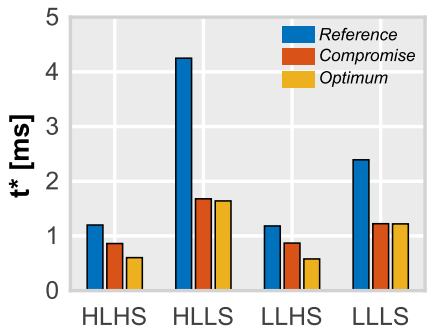

Fig. 14. Comparison of t* values for reference (blue), compromise (orange) and optimum pre-chambers (yellow) for each extreme operating condition. (For interpretation of the references to color in this figure legend, the reader is referred to the web version of this article.)

for optimizing the combustion phasing and therefore resulting in an efficiency loss.

The addition of external EGR emerges as a possible solution to ensure a suitable combustion phasing at these conditions while widening the operating limits. However, the combination of less fuel available at the start of ejection and the lower burning rates inside the pre-chamber decreases the performance of the hot-gas ejection process.

Therefore, the pre-chamber geometry should be optimized to improve the quality of the ejected jets. For this purpose, a set of 1-D calculations were performed using simplified numerical tools. The optimization results revealed different trends depending on the operating point considered. Thus, a compromise pre-chamber design should be chosen to assure a suitable operation in the whole engine map. This new pre-chamber showed a relevant improvement in terms of jet performance. A decrease of 50% in t* values is observed for the low engine speed cases, and around 30% of reduction for the high engine speed cases.

In light of these results, further research is needed to design the internal geometry of the proposed pre-chamber configuration through advanced numerical methods (CFD) and engine testing.

CRediT authorship contribution statement

R. Novella: Conceptualization, Funding acquisition, Supervision. **J. Gomez-Soriano:** Project administration, Supervision, Writing – original draft, Writing – review & editing. **I. Barbery:** Conceptualization, Methodology, Writing – original draft, Writing – review & editing. **P.J. Martinez-Hernandiz:** Data curation, Software, Validation, Writing – original draft.

Declaration of competing interest

The authors declare that they have no known competing financial interests or personal relationships that could have appeared to influence the work reported in this paper.

Data availability

The authors do not have permission to share data.

Acknowledgments

The work has been partially supported by the Spanish Ministerio de Economía *y* Competitividad, Spain through grant number TRA2017-89139-C2-1-R. The authors also wish to thank Mr. Gabriel Alcantarilla for his inestimable assistance during the experimental campaign.

References

[1] Heywood JB, et al. Internal combustion engine fundamentals. Mcgraw-hill New York; 1988.

[2] Payri González F, Desantes Fernández JM. Motores de combustión interna alternativos. Colección Acad. Editorial UPV 2011.

[3] Grandin B, Denbratt I. The effect of knock on heat transfer in SI engines. In: SAE 2002 world congress & exhibition. SAE International; 2002, http://dx.doi.org/10.4271/2002-01-0238.

[4] Yu S, Zheng M. Future gasoline engine ignition: A review on advanced concepts. Int J Engine Res 2021;22(6):1743–75.

[5] Attard WP, Blaxill H, Anderson EK, Litke P. Knock limit extension with a gasoline fueled pre-chamber jet igniter in a modern vehicle powertrain. SAE Int J Engines 2012;5(3):1201–15. http://dx.doi.org/10.4271/2012-01-1143.

[6] Feng H, Suo X, Xiao S, Chen X, Zhang Z, Gao N, et al. Numerical simulation on the effects of n-butanol combined with intake dilution on engine knock. Energy 2023;271:126918.

[7] Divekar P, Han X, Zhang X, Zheng M, Tjong J. Energy efficiency improvements and CO2 emission reduction by CNG use in medium-and heavy-duty spark-ignition engines. Energy 2023;263:125769.

[8] Szybist J. Knock mitigation effectiveness of EGR across the pressure-temperature domain. In: SAE powertrains, fuels & lubricants meeting. SAE International; 2020, http://dx.doi.org/10.4271/2020-01-2053.

[9] Diana S, Giglio V, Iorio B, Police G. Evaluation of the effect of EGR on engine knock. In: International fall fuels and lubricants meeting and exposition. SAE International; 1998, http://dx.doi.org/10.4271/982479.

[10] Toulson E, Schock HJ, Attard WP. A review of pre-chamber initiated jet ignition combustion systems. In: SAE 2010 powertrains fuels & lubricants meeting. SAE International; 2010, http://dx.doi.org/10.4271/2010-01-2263.

[11] Alvarez CEC, Couto GE, Roso VR, Thiriet AB, Valle RM. A review of prechamber ignition systems as lean combustion technology for SI engines. Appl Therm Eng 2018;128:107–20. http://dx.doi.org/10.1016/j.applthermaleng.2017.08.118, URL http://www.sciencedirect.com/science/article/pii/S1359431117302284.

[12] Attard WP, Fraser N, Parsons P, Toulson E. A turbulent jet ignition pre-chamber combustion system for large fuel economy improvements in a modern vehicle powertrain. SAE Int J Engines 2010;3(2):20–37. http://dx.doi.org/10.4271/2010-01-1457.

[13] Attard WP, Blaxill H. A single fuel pre-chamber jet ignition powertrain achieving high load, high efficiency and near zero NOx emissions. SAE Int J Engines 2011;5(3):734–46. http://dx.doi.org/10.4271/2011-01-2023.

[14] Attard WP, Blaxill H. A lean burn gasoline fueled pre-chamber jet ignition combustion system achieving high efficiency and low NOx at part load. In: SAE 2012 world congress & exhibition. SAE International; 2012, http://dx.doi.org/10.4271/2012-01-1146.

[15] Benajes J, Novella R, Gomez-Soriano J, Martinez-Hernandiz P, Libert C, Dabiri M. Evaluation of the passive pre-chamber ignition concept for future high compression ratio turbocharged spark-ignition engines. Appl Energy 2019;248:576–88. http://dx.doi.org/10.1016/j.apenergy.2019.04.131, URL http://www.sciencedirect.com/science/article/pii/S030626191930769X.

[16] Gentz G, Gholamisheeri M, Toulson E. A study of a turbulent jet ignition system fueled with iso-octane: Pressure trace analysis and combustion visualization. Appl Energy 2017;189:385–94. http://dx.doi.org/10.1016/j.apenergy.2016.12.055, URL http://www.sciencedirect.com/science/article/pii/S0306261916318189.

[17] Toulson E, Huisjen A, Chen X, Squibb C, Zhu G, Schock H, et al. Visualization of propane and natural gas spark ignition and turbulent jet ignition combustion. SAE Int J Engines 2012;5(4):1821–35. http://dx.doi.org/10.4271/2012-32-0002.

[18] Di Sabatino F, Martinez-Hernandiz PJ, Novella Rosa R, Ekoto I. Investigation of the effects of passive pre-chamber nozzle pattern and ignition system on engine performance and emissions. Int J Engine Res 2022;14680874221129331.

[19] Xu G, Wright YM, Schiliro M, Boulouchos K. Characterization of combustion in a gas engine ignited using a small un-scavenged pre-chamber. Int J Engine Res 2020;21(7):1085–106.

[20] Gentz G, Thelen B, Gholamisheeri M, Litke P, Brown A, Hoke J, et al. A study of the influence of orifice diameter on a turbulent jet ignition system through combustion visualization and performance characterization in a rapid compression machine. Appl Therm Eng 2015;81:399–411. http://dx.doi.org/10.1016/j.applthermaleng.2015.02.026, URL http://www.sciencedirect.com/science/article/pii/S1359431115001349.

[21] Gholamisheeri M, Wichman IS, Toulson E. A study of the turbulent jet flow field in a methane fueled turbulent jet ignition (TJI) system. Combust Flame 2017;183:194–206. http://dx.doi.org/10.1016/j.combustflame.2017.05.008, URL http://www.sciencedirect.com/science/article/pii/S001021801730175X.

[22] Vedula RT, Song R, Stuecken T, Zhu GG, Schock H. Thermal efficiency of a dual-mode turbulent jet ignition engine under lean and near-stoichiometric operation. Int J Engine Res 2017;18(10):1055–66. http://dx.doi.org/10.1177/1468087417699979.

[23] Xu G, Kotzagianni M, Kyrtatos P, Wright YM, Boulouchos K. Experimental and numerical investigations of the unscavenged prechamber combustion in a rapid compression and expansion machine under engine-like conditions. Combust Flame 2019;204:68–84. http://dx.doi.org/10.1016/j.combustflame.2019.01.025, URL http://www.sciencedirect.com/science/article/pii/S0010218019300434.

[24] Mastorakos E, Allison P, Giusti A, De Oliveira P, Benekos S, Wright Y, et al. Fundamental aspects of jet ignition for natural gas engines. SAE In J Engines 2017. http://dx.doi.org/10.4271/2017-24-0097.

[25] Allison P, de Oliveira M, Giusti A, Mastorakos E. Pre-chamber ignition mechanism: Experiments and simulations on turbulent jet flame structure. Fuel 2018;230:274–81. http://dx.doi.org/10.1016/j.fuel.2018.05.005, URL http://www.sciencedirect.com/science/article/pii/S0016236118308287.

[26] Bunce M, Blaxill H. Methodology for combustion analysis of a spark ignition engine incorporating a pre-chamber combustor. In: SAE 2014 international powertrain, fuels & lubricants meeting. SAE International; 2014, http://dx.doi.org/10.4271/2014-01-2603.

[27] Benajes J, Novella R, Gomez-Soriano J, Barbery I, Libert C, Rampanarivo F, et al. Computational assessment towards understanding the energy conversion and combustion process of lean mixtures in passive pre-chamber ignited engines. Appl Therm Eng 2020;178:115501. http://dx.doi.org/10.1016/j.applthermaleng.2020.115501, URL http://www.sciencedirect.com/science/article/pii/S1359431120329835.

[28] Benajes J, Novella R, Gomez-Soriano J, Barbery I, Libert C. Advantages of hydrogen addition in a passive pre-chamber ignited si engine for passenger car applications. Int J Energy Res 2021;45(9):13219–37.

[29] Thelen BC, Toulson E. A computational study on the effect of the orifice size on the performance of a turbulent jet ignition system. Proc Inst Mech Eng D 2017;231(4):536–54.

[30] Biswas S, Qiao L. Ignition of ultra-lean premixed H2/air using multiple hot turbulent jets generated by pre-chamber combustion. Appl Therm Eng 2018;132:102–14. http://dx.doi.org/10.1016/j.applthermaleng.2017.11.073, URL http://www.sciencedirect.com/science/article/pii/S1359431117353000.

[31] Biswas S, Qiao L. Ignition of ultra-lean premixed hydrogen/air by an impinging hot jet. Appl Energy 2018;228:954–64.

[32] Onofrio G, Napolitano P, Tunestål P, Beatrice C. Combustion sensitivity to the nozzle hole size in an active pre-chamber ultra-lean heavy-duty natural gas engine. Energy 2021;235:121298.

[33] Yang X, Cheng Y, Wang P. The scavenging timing of pre-chamber on the performance of a natural gas engine. Int J Engine Res 2021;22(9):2919–30.

[34] Kim J, Scarcelli R, Som S, Shah A, Biruduganti MS, Longman DE. Numerical investigation of a fueled pre-chamber spark-ignition natural gas engine. Int J Engine Res 2022;23(9):1475–94.

[35] Zardoya AR, Lucena IL, Bengoetxea IO, Orosa JA. Research on an internal combustion engine with an injected pre-chamber to operate with low methane number fuels for future gas flaring reduction. Energy 2022;253:124096.

[36] Zardoya AR, Lucena IL, Bengoetxea IO, Orosa JA. Research on the new combustion chamber design to operate with low methane number fuels in an internal combustion engine with pre-chamber. Energy 2023;275:127458.

[37] Payri R, Novella R, Barbery I, Bori-Fabra O. Numerical and experimental evaluation of the passive pre-chamber concept for future CNG SI engines. Appl Therm Eng 2023;230:120754.

[38] Atis CAA, Ayele Y, Stuecken T, Schock H. Effect of pre-chamber scavenging strategy on EGR tolerance and thermal efficiency of pre-chamber turbulent jet ignition systems. Int J Engine Res 2022;14680874221105162.

[39] Rohwer J, Han T, Shah A, Rockstroh T. Investigations into EGR dilution tolerance in a pre-chamber ignited GDI engine. Int J Engine Res 2022;14680874221084777.

[40] Novella R, Gomez-Soriano J, Barbery I, Libert C. Numerical analysis of the passive pre-chamber ignition concept for light duty applications. Appl Therm Eng 2022;213:118610.

[41] Novella R, Pastor J, Gomez-Soriano J, Barbery I, Libert C, Rampanarivo F, et al. Experimental and numerical analysis of passive pre-chamber ignition with EGR and air dilution for future generation passenger car engines. Tech. rep., SAE Technical Paper; 2020.

[42] Yontar AA. A comparative study to evaluate the effects of pre-chamber jet ignition for engine characteristics and emission formations at high speed. Energy 2020;210:118640.

[43] López J, Novella R, Gomez-Soriano J, Martinez-Hernandiz P, Rampanarivo F, Libert C, et al. Advantages of the unscavenged pre-chamber ignition system in turbocharged natural gas engines for automotive applications. Energy 2021;218:119466. http://dx.doi.org/10.1016/j.energy.2020.119466, URL http://www.sciencedirect.com/science/article/pii/S0360544220325731.

[44] Lapuerta M, Armas O, Hernández J. Diagnosis of DI diesel combustion from in-cylinder pressure signal by estimation of mean thermodynamic properties of the gas. Appl Therm Eng 1999;19(5):513–29. http://dx.doi.org/10.1016/S1359-4311(98)00075-1, URL http://www.sciencedirect.com/science/article/pii/S1359431198000751.

[45] Payri F, Molina S, Martín J, Armas O. Influence of measurement errors and estimated parameters on combustion diagnosis. Appl Therm Eng 2006;26(2):226–36. http://dx.doi.org/10.1016/j.applthermaleng.2005.05.006, URL http://www.sciencedirect.com/science/article/pii/S1359431105001560.

[46] García-Oliver J, Niki Y, Rajasegar R, Novella R, Gomez-Soriano J, Martínez-Hernándiz P, et al. An experimental and one-dimensional modeling analysis of turbulent gas ejection in pre-chamber engines. Fuel 2021;299:120861. http://dx.doi.org/10.1016/j.fuel.2021.120861, URL https://www.sciencedirect.com/science/article/pii/S0016236121007389.

[47] Pastor JV, López JJ, García JM, Pastor JM. A 1D model for the description of mixing-controlled inert diesel sprays. Fuel 2008;87(13):2871–85. http://dx.doi.org/10.1016/j.fuel.2008.04.017, URL http://www.sciencedirect.com/science/article/pii/S0016236108001580.

[48] Desantes J, Pastor J, García-Oliver J, Pastor J. A 1D model for the description of mixing-controlled reacting diesel sprays. Combust Flame 2009;156(1):234–49. http://dx.doi.org/10.1016/j.combustflame.2008.10.008, URL http://www.sciencedirect.com/science/article/pii/S0010218008003088.

[49] Desantes J, García-Oliver J, Xuan T, Vera-Tudela W. A study on tip penetration velocity and radial expansion of reacting diesel sprays with different fuels. Fuel 2017;207:323–35. http://dx.doi.org/10.1016/j.fuel.2017.06.108, URL http://www.sciencedirect.com/science/article/pii/S0016236117308177.

[50] Novella R, Gomez-Soriano J, Martinez-Hernandiz P, Libert C, Rampanarivo F. Improving the performance of the passive pre-chamber ignition concept for spark-ignition engines fueled with natural gas. Fuel 2021;290:119971. http://dx.doi.org/10.1016/j.fuel.2020.119971, URL https://www.sciencedirect.com/science/article/pii/S0016236120329677.

[51] Climent H, Dolz V, Pla B, González-Domínguez D. Analysis on the potential of EGR strategy to reduce fuel consumption in hybrid powertrains based on advanced gasoline engines under simulated driving cycle conditions. Energy Convers Manage 2022;266:115830.

[52] Benajes J, Novella R, Gomez-Soriano J, Martinez-Hernandiz P, Libert C, Dabiri M. Performance of the passive pre-chamber ignition concept in a spark-ignition engine for passenger car applications. In: SIA powertrain & electronics. 2019.